Behavioural Brain Research 322 (2017) 339–350

Contents lists available at ScienceDirect

Behavioural Brain Research

journal homepage: www.elsevier.com/locate/bbr

Research report

Classification of patients with MCI and AD from healthy controls using directed graph measures of resting-state fMRI

Ali Khazaee[a], Ata Ebrahimzadeh[b], Abbas Babajani-Feremi[c,d,e,*], for the Alzheimer's Disease Neuroimaging Initiative[1]

[a] Department of Electrical Engineering, University of Bojnord, Bojnord, Iran
[b] Department of Electrical Engineering, Babol University of Technology, Babol, Iran
[c] Department of Pediatrics, Division of Clinical Neurosciences, University of Tennessee Health Science Center, Memphis, TN, USA
[d] Neuroscience Institute, Le Bonheur Children's Hospital, Memphis, TN, USA
[e] Department of Anatomy and Neurobiology, University of Tennessee Health Science Center, Memphis, TN, USA

HIGHLIGHTS

- We used directed graph measures to identify alteration of brain network in MCI and AD.
- We achieved an accuracy of 93.3% for classification of AD, MCI, and control subjects.
- AD Patients may experience disappearing some hub regions during disease progression.
- Directed graph measures of rs-fMRI data can be used to identify the early stage of AD.

ARTICLE INFO

Article history:
Received 15 March 2016
Received in revised form 21 June 2016
Accepted 23 June 2016
Available online 23 June 2016

Keywords:
Alzheimer's disease (AD)
Mild cognitive impairment (MCI)
Resting-state fMRI
Granger causality analysis
Graph theoretical approach
Machine learning approach

ABSTRACT

Brain network alterations in patients with Alzheimer's disease (AD) has been the subject of much investigation, but the biological mechanisms underlying these alterations remain poorly understood. Here, we aim to identify the changes in brain networks in patients with AD and mild cognitive impairment (MCI), and provide an accurate algorithm for classification of these patients from healthy control subjects (HC) by using a graph theoretical approach and advanced machine learning methods. Multivariate Granger causality analysis was performed on resting-state functional magnetic resonance imaging (rs-fMRI) data of 34 AD, 89 MCI, and 45 HC to calculate various directed graph measures. The graph measures were used as the original feature set for the machine learning algorithm. Filter and wrapper feature selection methods were applied to the original feature set to select an optimal subset of features. An accuracy of 93.3% was achieved for classification of AD, MCI, and HC using the optimal features and the naïve Bayes classifier. We also performed a hub node analysis and found that the number of hubs in HC, MCI, and AD were 12, 10, and 9, respectively, suggesting that patients with AD experience disturbance of critical communication areas in their brain network as AD progresses. The findings of this study provide insight into the neurophysiological mechanisms underlying MCI and AD. The proposed classification method highlights the potential of directed graph measures of rs-fMRI data for identification of the early stage of AD.

* Corresponding author at: Department of Pediatrics, Division of Clinical Neurosciences, The University of Tennessee Health Science Center, Neuroscience Institute, Le Bonheur Children's Hospital, 51 N Dunlap St., Suite P320, Memphis, TN 38105, USA.
E-mail addresses: ababajan@uthsc.edu, ababajani@yahoo.com (A. Babajani-Feremi).

[1] Data used in preparation of this article were obtained from the Alzheimer's Disease Neuroimaging Initiative (ADNI) database (adni.loni.usc.edu). As such, the investigators within the ADNI contributed to the design and implementation of ADNI and/or provided data but did not participate in analysis or writing of this report. A complete listing of ADNI investigators can be found at: http://adni.loni.usc.edu/wp-content/uploads/how_to_apply/ADNI_Acknowledgement_List.pdf.

http://dx.doi.org/10.1016/j.bbr.2016.06.043
0166-4328/

1. Introduction

Alzheimer's disease (AD) is a neurodegenerative disorder characterized by dementia and cognitive decline [7]. Mild cognitive impairment (MCI) is an intermediate disease stage before the onset of early AD, and subjects with MCI are of high risk developing AD [68]. Various studies describe AD as a disconnection syndrome, due to observed alterations in functional and structural connectivity of brain regions [1,21,38], and it has been demonstrated that patients with MCI and AD have alteration in functional, regional, and whole brain connectivity [71,73,81,99].

Recently, resting-state functional magnetic resonance imaging (rs-fMRI) has been widely used to study MCI and AD [2,4,5,14,38,55,58,71,81,88,89,98]. Many studies analyze rs-fMRI data by calculating the Pearson's correlation coefficient to define the functional connectivity of brain regions. Since functional connectivity provides no information about directional interactions between the brain networks, it has been suggested that effective connectivity, which reveals the direction of information flow between different brain regions, may provide new insights into the underlying neuronal alterations in MCI and AD [23].

Previous studies employed the effective connectivity using multivariate Granger causality to investigate alterations in brain networks in MCI and AD [30,57,61,63,93]. Miao et al. [63] investigated the causal interactions between nodes in default mode network (DMN) and reported disruption in causal interaction between medial prefrontal cortex (mPFC) and inferior parietal cortex (IPC) with other nodes in the DMN. In another study, Liu et al. [61] found that causal interactions among resting state networks (RSNs) decreased in patients with AD as compared to healthy controls. They also found that the causal interactions between the default mode network and auditory network were weaker in patients with AD, but the causal interactions between the executive control network and the memory network were stronger in these patients. Wen et al. investigated the causal interactions between eight core regions in DMN and found decreased Granger causal influence in mPFC [93]. Liang et al. [57] concentrated on effective connectivity of four important RSNs, *i.e.* DMN, hippocampal cortical memory network, dorsal attention network, and frontoparietal control network, in amnestic MCI (aMCI) patients. They found that the causal interactions between different areas in four RSNs were significantly altered in aMCI patients as compared to healthy controls. They observed both increases and decreases in the causal interactions between different areas in aMCI patients, and suggested coexistence of causal compensation and disconnection in these patients. Overall, previous studies have provided some evidence that the Granger causality analysis of rs-fMRI data has value in MCI and AD applications. However, the number of these studies is relatively small and their results are not consistent. To address this, we investigated efficacy of the Granger causality analysis to identify alteration of the brain network in patients with MCI and AD.

To date, several studies have employed machine learning approaches for automatic identification of patients with MCI and AD [15,19], and some also performed classification of these patients using undirected graph measures [45,46,48–50,56,87,91]. Undirected graph measures may not be able to adequately characterize the information flow among the regions within the brain network. In the current study, we employed the Granger causality to account for directional interactions between brain regions. To the best of our knowledge, there is no study to use directed graph measures for identification of MCI and AD. The main goal of the current study was to develop and evaluate an accurate and automated method for classification of AD, MCI, and healthy control (HC) using directed graph measures.

2. Materials and methods

2.1. Patients

The rs-fMRI data of 34 patients with AD (average age 72.5 years, 18 female), 89 patients with MCI (average age 71.8 years, 46 female), and 45 HC subjects (average age 75.9 years, 26 female) were analyzed in this study (Table 1). All subjects were selected from the Alzheimer's disease neuroimaging initiative (ADNI) database.[2] Patients with AD had a Mini-Mental State Examination (MMSE) score of 14–26, a Clinical Dementia Rating (CDR) of 0.5 or 1.0, and met the National Institute of Neurological and Communicative Disorders and Stroke and the Alzheimer's Disease and Related Disorders Association (NINCDS/ADRDA) criteria for probable AD. Patients with MCI had MMSE scores between 24 and 30, a memory complaint, objective memory loss measured by education adjusted scores on Wechsler Memory Scale Logical Memory II, a CDR of 0.5, absence of significant levels of impairment in other cognitive domains, essentially preserved activities of daily living, and an absence of dementia. The HC subjects were non-depressed, non-MCI, non-demented, and had a MMSE score of 24–30 and a CDR of 0.

2.2. Data acquisition and preprocessing

Functional and structural MRI data were collected according to the ADNI acquisition protocol using three tesla (3T) scanner [44]. The rs-fMRI data in each subject consisted of 140 functional volumes and acquired with following parameters: repetition time (TR) = 3000 ms; echo time (TE) = 30 ms; flip angle = 80°; slice thickness = 3.313 mm; and 48 slices. Preprocessing of rs-fMRI data were detailed elsewhere [48]. Briefly, the preprocessing steps were as follows: leaving the first few volumes (7 vol) of the functional images for signal equilibrium and participant's adaptation to the circumstances; slice-timing correction to the last slice; realignment for head movement compensation by using a six-parameter rigid-body spatial transformation [33]; normalization to the Montreal Neurological Institute (MNI) space; resampling to 3-mm isotropic voxels; detrending; smoothing using a Gaussian filter with full width at half maximum (FWHM) of 4 mm; and band-pass filtering (0.01–0.08 Hz). During the realignment step, four subjects (two normal, one MCI, and one AD) exhibited excessive head motion and were excluded from further analysis. The whole-brain signal was removed by a multiple linear regression analysis [29,31,37] to reduce the effect of the physiological artifacts. To reduce the effects of motion and non-neuronal blood oxygen level-dependent (BOLD) fluctuations, head motion as well as the cerebrospinal fluid (CSF) and white matter signals were removed as nuisance covariates [29,47]. Preprocessing of rs-fMRI data was carried out using the Data Processing Assistant for Resting-State fMRI (DPARSF) toolbox [16] and the SPM5 package (http://www.fil.ion.ucl.ac.uk/spm).

2.3. Brain network analysis

The 264 putative functional area atlas [70] was employed to parcellate the brain. These areas were formed by applying two methods of meta-analytic and functional connectivity mapping to the rs-

[2] Data used in the preparation of this article were obtained from the Alzheimer's Disease Neuroimaging Initiative (ADNI) database (adni.loni.usc.edu). The ADNI was launched in 2003 as a public-private partnership, led by Principal Investigator Michael W. Weiner, MD. The primary goal of ADNI has been to test whether serial magnetic resonance imaging (MRI), positron emission tomography (PET), other biological markers, and clinical and neuropsychological assessment can be combined to measure the progression of mild cognitive impairment (MCI) and early Alzheimer's disease (AD). For up-to-date information, see www.adni-info.org.

Table 1
Demographic and behavioral information. MMSE: Mini-Mental State Examination; CDR: Clinical Dementia Rating.

	Healthy Controls (HC)	Patients with MCI	Patients with AD
Number	45	89	34
Male/Female	19/26	43/46	16/18
Age (Mean ± STD) years	75.90 ± 6.79	71.77 ± 7.78	72.54 ± 7.02
MMSE score (Mean ± STD)	28.95 ± 1.56	27.56 ± 2.20	21.24 ± 3.37
CDR score (Mean ± STD)	0.07 ± 0.21	0.49 ± 0.17	0.92 ± 0.31

fMRI data [70]. The time series of voxels within each of 264 regions of interest (ROIs) were averaged to generate a representative signal for each ROI. We also used the automated anatomical atlas (AAL) parcellation [83], which is widely used in neuroimaging research. We averaged signals in each of the 90 ROIs of AAL atlas and 90 time series for each subject were obtained. To construct a directed brain network, connectivity among ROIs were calculated using the Granger causality analysis. Multivariate Granger causality coefficients of each pair of ROIs were calculated using mvgc toolbox [79]. Bivariate Granger causality of two time series $X_1(t)$ and $X_2(t)$ can be formulated by an autoregressive model:

$$X_1(t) = \sum_{i=1}^{p} A_{11,i} X_1(t-i) + \sum_{i=1}^{p} A_{12,i} X_2(t-i) + E_1(t) \quad (1)$$

$$X_2(t) = \sum_{i=1}^{p} A_{21,i} X_1(t-i) + \sum_{i=1}^{p} A_{22,i} X_2(t-i) + E_2(t) \quad (2)$$

where p is the model order, *i.e.* the maximum number of lagged samples, A_{ij} are coefficients of model, and $E_1(t)$ and $E_2(t)$ are the prediction residual errors. If inclusion of X_2 in the first equation improves prediction of X_1 by reducing the variance of E_1, then it is said that X_2 causes X_1, and vice versa [36]. Multivariate Granger causality is a generalization of the above bivariate model by including more than two variables in a multivariate autoregressive (MVAR) model [35].

It is noteworthy that a challenging issue in MVAR model is to find correct model order. If the model order is too low, the model cannot capture the essential dynamics of the data and accuracy of the prediction will be low. If the model order is too high, the model over-fits noise and unwanted signals, the generality of model decreases, and instabilities occur. Several criteria, such as Bayesian information criteria (BIC) [77] and Akaike information criterion (AIC) [92], have been proposed for calculating an optimal model order. We used the BIC to estimate the model order of a MVAR with 264 variables in the current study. To model causal interactions among the rs-fMRI time series of ROIs, A directed graph with 264 nodes were constructed for each subject. For further analysis, we converted the directed graphs to sparse ones by thresholding the graph at an optimal threshold value [24]. We found an optimal value for threshold by maximizing the global cost efficiency [48]. The binary directed connectivity matrix for each subject was calculated by thresholding the connectivity matrix and setting its diagonal elements to zero. It is noteworthy that some nodes may be disconnected after thresholding that causes difficulties in calculation of some graph measures, *e.g.* characteristic path length. To overcome this problem, we preserved the connecting edge between two disconnected regions even if its weight is below the threshold value. Adding edges in some subjects leads to different number of edges in them. To ensure that graphs in all subjects had the same number of edges after thresholding, we eliminated one edge per two disconnected regions in a graph. When we added a connecting edge to connect a disconnected sub-graph, we then eliminated one edge from the original graph to preserve the same number of edges in all subjects. We had 264 nodes and 69,432 (264*263) directed edges. 11,803 directed edges were retained after thresholding at 17%. If we had, for example, one disconnected sub-graph in a subject, we would add one edge to connect this sub-graph to the main graph. Consequently, we had 11,804 edges in this subject, one edge more than other subjects. To correct this problem, we first eliminated the edge with the lowest weight from 11,803 edges and then added one connecting edge. In the same manner, if we had n disconnected sub-graphs, we would eliminate n edges with the lowest weight from the original 11,803 edges and then add n connecting edges.

2.4. Computation of graph measures

The binary directed connectivity matrix for each subject was used to calculate the following graph measures: degree (in-degree and out-degree), betweenness centrality [51], flow coefficient [43], local efficiency [54], K-coreness centrality [39], pagerank centrality [9], node strength, clustering coefficient [28], global efficiency [54], characteristic path length [75,90], range coefficient [90], transitivity [28], and assortativity [65]. It is noteworthy that some of these graph measures are global, *i.e.* they have one value in each subject, and some of them are local measures, *i.e.* they have one value for each brain region in each subject. Global measures were clustering coefficient, global efficiency, characteristic path length, range coefficient, transitivity, and assortativity. All graph measures were calculated using Brain Connectivity Toolbox (BCT) [74].

2.5. Feature selection and classification

A feature vector, with a large amount of features, was generated based on the local and global graph measures. Dealing with large size feature vectors is challenging, and feature selection is an essential stage in the classification algorithm. High dimensionality of feature space increases the complexity of the model and results in increased training and testing time, and redundancy in features degrades the performance of model estimation. Here, a combination of filter and wrapper feature selection algorithms were used to select optimal features. First, a filter feature selection algorithm, *i.e.* Fisher algorithm [27], was used to sort all features based on their individual discrimination ability. Then the first half of the best features with the highest discrimination ability was selected and the wrapper feature selection algorithm was applied to them. The wrapper algorithm was implemented using the forward sequential feature selection (FSFS) method and 10 fold cross-validation.

An optimal subset of features was selected using supervised classifiers. Different supervised classifiers, including support vector machine (SVM) and naïve Bayes classifier, have been used in neuroimaging literature. We examined these classifiers and most appropriate for our study was the naïve Bayes classifier. The naïve Bayes classifier assumes that features are conditionally independent within each class. This assumption simplifies the training step because the density can be calculated individually for each feature. The naïve Bayes classifier has been shown to be remarkably successful in practice, though its independence assumption is unrealistic [25,41,64,72]. Surprisingly effective performance of the naïve Bayes classifier despite its unrealistic independence assumption may be related to the fact that it regularly allocates maximum probability to the correct class even if its probability estimates are imprecise [72]. A ten-fold cross validation strategy was employed for robust classification. The performance of classification was

Table 2
Performance of classification using naïve Bayes and SVM with radial base function (RBF) kernel.

Classifier	Accuracy	Sensitivity			Specificity			Positive predictivity		
		HC	MCI	AD	HC	MCI	AD	HC	MCI	AD
SVM (RBF)	71.95	53.1	86.4	51.5	88.4	61.8	97.7	64	72.4	85
Naïve Bayes	93.29	88.4	100	81.8	100	85.5	100	100	88.9	100

Table 3
Performance of classification using each group of features. In every classification phase, all steps of algorithm were performed except that only one graph measure were used as feature set. Local graph measures had 264 feature values while global graph measures had one feature value.

		Number of selected features	Accuracy (%)
Local graph measures (each group has 264 features)	Betweenness centrality	57	79.4
	Pagerank centrality	92	76.8
	Outdegree	91	72.7
	Total flow	27	71.4
	Local efficiency	8	66.6
	Flow coefficient	66	66.0
	Indegree	73	62.9
	K-coreness centrality	9	62.8
	Degree (Indegree+ Outdegree)	11	62.2
	Node strength	3	59.1
	Local/Global efficiency	1	55.0
Global graph measures (each group has a single feature)	Assortativity in-degree/in-degree	1	53.8
	Transitivity	1	53.2
	Clustering coefficient	1	53.1
	Characteristic path length	1	53.1
	Assortativity out-degree/in-degree	1	53.1
	Assortativity in-degree/out-degree	1	53.1
	fraction of shortcuts in the graph	1	52.5
	Assortativity out-degree/out-degree	1	51.3
	Global efficiency	1	50.0
	Average range for entire graph	1	26.2
	All 2914 features	340	93.3

evaluated using accuracy, sensitivity, specificity, and positive predictivity measures.

2.6. Overall procedure

The overall procedure of this study is shown in Fig. 1. The main procedural steps are related to automatic classification of AD, MCI and HC groups, and are depicted by vertical arrows in Fig. 1. Sub-procedures, were performed to identify alterations of the brain networks in MCI and AD, are linked by horizontal arrows in Fig. 1. As shown in Fig. 1, after preprocessing of rs-fMRI data, a functional area atlas was used to parcellate the brain to 264 nodes. Directed connections corresponding to each pair of 264 areas were calculated using the Granger causality analysis and used as the graph edges. Consequently, a dense directed connectivity matrix was constructed for each subject. Previous studies have shown that graph measures are threshold-dependent and the values of graph measures may vary in different threshold values [34]. Based on methods described in Section 2.3, the dense directed connectivity matrix was converted to sparse matrix using an optimal proportional threshold value of 0.17, by retaining only 17% of the strongest edges (Fig. 2). As mentioned in Section 2.3, we found an optimal value for threshold (17%) by maximizing the global cost efficiency. It was shown that maximizing the global cost efficiency is a robust method for finding an optimal value for threshold [24,48]. Following this, 11 directed local graph measures and 10 directed global graph measures were calculated based on the sparse directed connectivity matrix. A combination of filter and wrapper feature selection algorithms were used to select an optimal subset of features from the original 2914 features, *i.e.* 264×11 local and 10 global features [48]. In the first step, a filter feature selection algorithm, *i.e.* Fisher algorithm, was used to sort 2914 features based on their individual discrimination ability. It is noteworthy that the filter feature selection algorithm does not need a cross-validation. In the next step, top 50% of features with highest Fisher score were selected and the wrapper feature selection algorithm was applied to them. The wrapper algorithm was implemented using the forward sequential feature selection (FSFS) method and 10-fold cross validation.

Hub nodes in the brain are important regions that play a central role in overall organization of the brain network [84]. Reorganization of the brain networks in patients with MCI and AD may eliminate or add some hub nodes to the network. We used degree of nodes (in-degree and out-degree) to identify the hub nodes in this study [12,61]. Nodes with a degree of two standard deviation higher than the mean of degree of all nodes were identified as hub nodes. Since the graph measures are threshold-dependent, we calculated the degree of nodes by varying the threshold in a range from 0.1 to 0.3 with a step of 0.01. For each value of threshold, the degree of nodes was calculated, and then hub nodes were identified. At the end of analysis, percentage of identification of a node as a hub node in different threshold values was calculated.

To understand alterations of the brain networks in patients with MCI and AD, another sub-procedure, based on the optimal subset of features, was performed. We selected features with high discriminative ability in identification of MCI and AD, and then identified the corresponding brain areas related to those features. These areas are expected to be the most affected cortical regions in patients with MCI and AD.

3. Results

Results of this study can be divided into two parts. In the first part (Section 3.1), we present results of an efficient algorithm for discrimination of patients with MCI and AD from HC subjects. The proposed algorithm used an optimal subset of features, which were extracted from the directed graph measures. In the second part

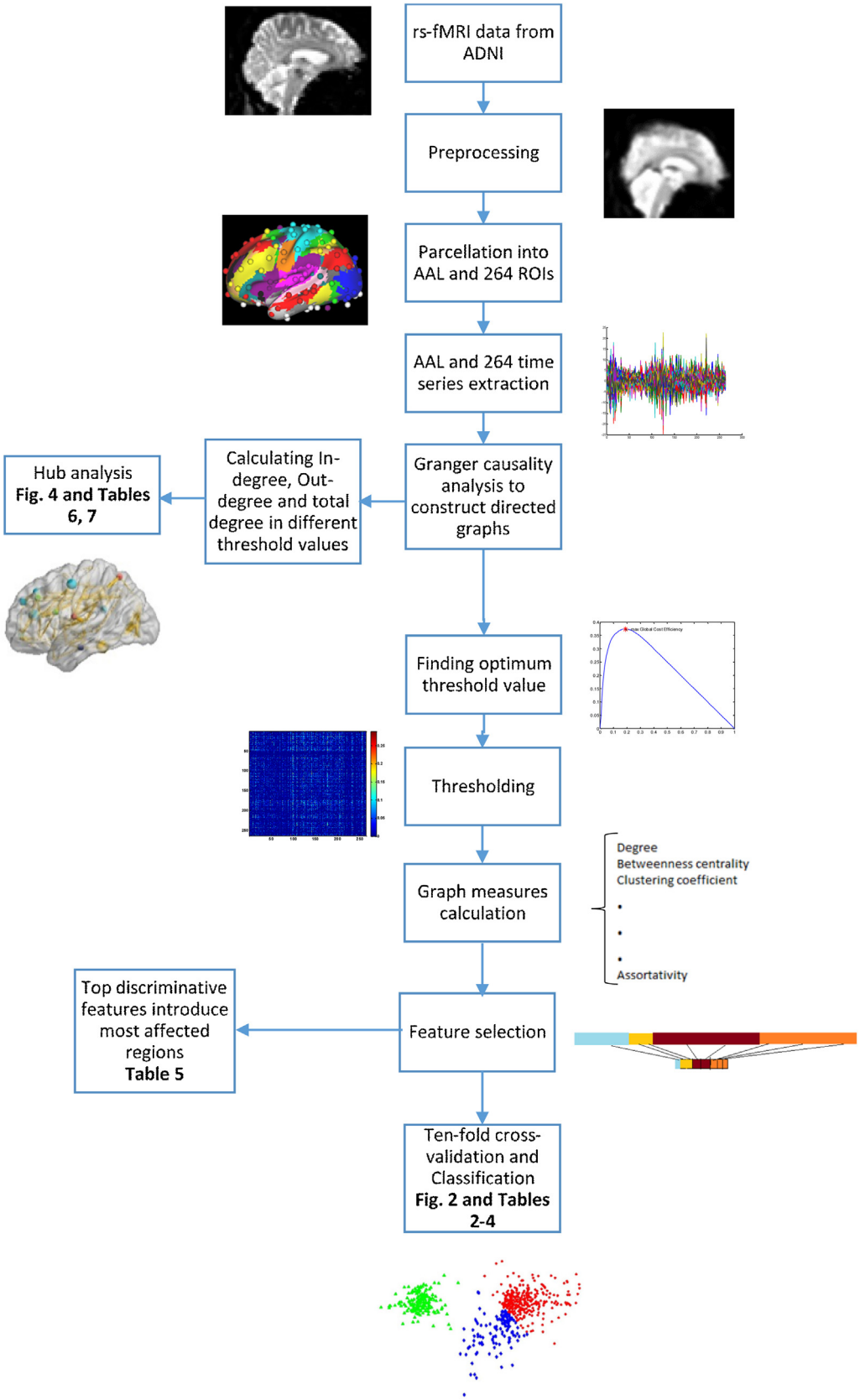

Fig 1. The overall procedure of this study.

(Section 3.2), the results of hub analysis for identification of alterations in the brain networks of patients with MCI and AD are presented.

3.1. Discrimination of patients with MCI and AD from HC

Various classifiers, such as linear discriminant analysis (LDA), K-nearest neighbor (KNN), decision trees, support vector machines

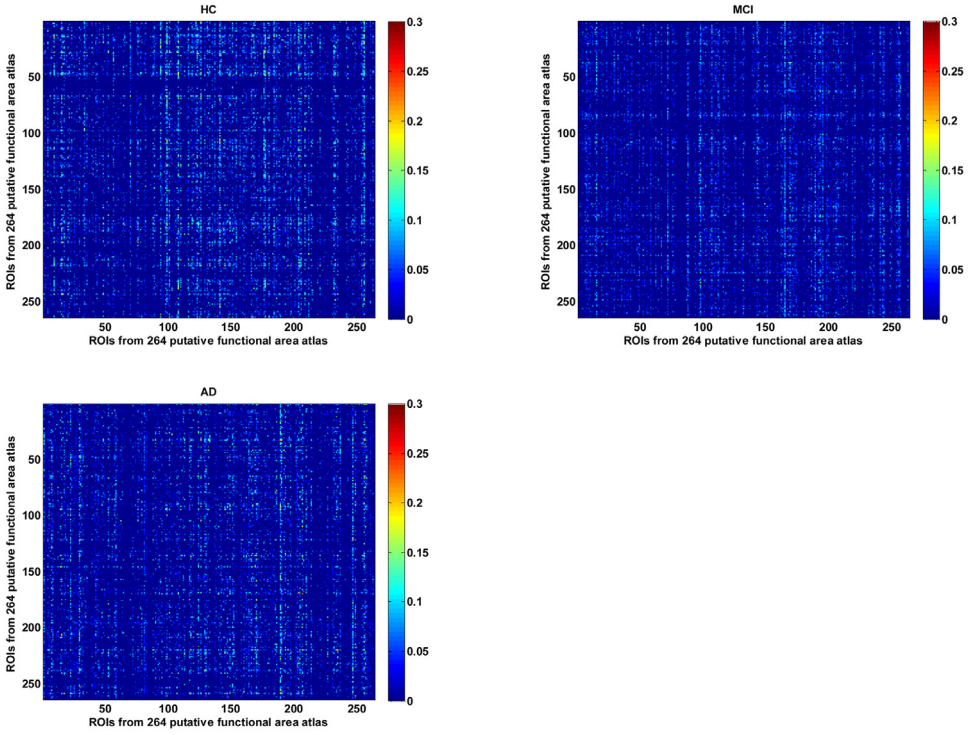

Fig. 2. Mean effective connectivity matrix of HC, MCI and AD. The matrices were thresholded at proportional threshold value of 0.17 by retaining only 17% of the strongest edges.

(SVM), and naïve Bayes, have been used in different neuroimaging applications. We examined performance of these classifiers for discrimination of patients with AD and MCI from HC subjects. The best performance was achieved using the naïve Bayes classifier. Performance of two best classifiers, *i.e.* naïve Bayes and SVM with radial base function (RBF) kernel, were compared using ten-fold cross validation strategy (Table 2). The naïve Bayes classifier outperformed the SVM classifier in all of the performance metrics and achieved a high accuracy of 93.3%. It is noteworthy that the naïve Bayes classifier provided 100% sensitivity in identification of MCI, *i.e.* all of patients with MCI were correctly classified. In addition, specificity of the naïve Bayes classifier in identification of AD and HC was 100%, *i.e.* there was no false positive in prediction of AD and HC.

Discrimination of MCI from HC is more difficult in comparison to classification of AD from HC. Several studies reported that they achieved good performance in discrimination of AD from HC [18,52], however, other studies have reported no significant difference between MCI and HC groups, or achieved a low performance in discrimination of these groups [18,53]. We investigated performance of classification of each pair of groups (*i.e.* HC *vs.* MCI, HC *vs.* AD, and MCI *vs.* AD) using the receiver operating characteristic (ROC) curves (Fig. 3). Area under the ROC curve (AUC) was calculated as a performance measure for each binary classification. The value of AUC for HC *vs.* MCI, MCI *vs.* AD, and HC *vs.* AD classification was 0.93, 0.90, and 0.94, respectively.

To investigate the discrimination ability of graph measures, we performed classification using only one graph measure and reported the results in Table 3. The best performance of individual graph measures was achieved using the betweenness centrality measure with 79.4% accuracy, followed by the pagerank centrality with 76.8% accuracy. We found that performance of the global graph measures was lower than that of the local graph measures. This finding is not surprising, because a global measure has only one feature per subject while a local graph measure has 264 features per subject. Nevertheless, accuracies of the global graph measures, which were approximately 50%, were still above the chance level (33.3%) for a three group classification. Assortativity related features were among the top global graph measures. Assortativity of a network represents tendency of its nodes to connect to others with similar degree (in-degree or out-degree). While no single graph measure achieved high accuracy in classification of AD, MCI, and HC, integration of all graph measures provided an accuracy of 93.3%. This result indicates that using one graph measure alone may not be sufficient to describe all aspects of the alterations in the brain networks of patients with MCI and AD. It is noteworthy that classification by integrating all graph measures was based on 340 optimal subset of original 2914 features.

Since the AAL atlas has been widely used in various rs-fMRI applications, we compared performance of this atlas and 264 putative functional area atlas (Table 4). The classification accuracy using the AAL and 264 putative functional area atlases was 79.9% and 93.3%, respectively. Performance of classification using AAL was degraded drastically in identification of AD where only 18 out of 33 patients with AD were classified correctly. In fact, the AAL and 264 putative functional area atlases achieved sensitivity of 54.5% and 81.8% in classification of AD, respectively. While identification of MCIs based on the 264 putative functional area atlas achieved 100% sensitivity, sensitivity of the AAL atlas was 88.6%.

The top 20 features corresponding to seven graph measures with maximum discrimination ability are listed in Table 5. Six graph measures were associated with two regions (left middle temporal gyrus and right medial superior frontal gyrus) in the DMN; four graph measures were associated with the left supplementary motor area (SMA) in the ventral attention network; three graph measures were associated with left inferior parietal gyrus and right superior parietal gyrus in the dorsal attention network; two graph measures were associated with each of the right postcentral gyrus, left superior occipital gyrus, and right inferior temporal gyrus; one graph measure, *i.e.* in-degree, was associated with the left rolandic operculum. Some regions have more than one associated graph

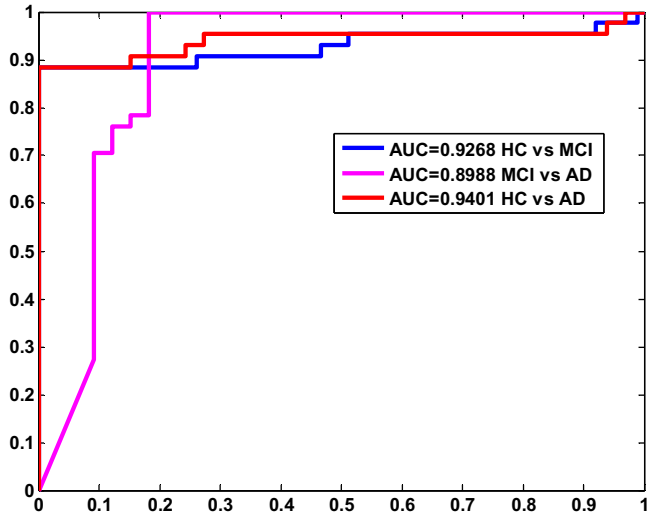

Fig. 3. ROC curves for binary classification of HC *vs.* MCI, MCI *vs.* AD, and HC *vs.* AD. Area under ROC curve (AUC) for each binary classification was indicated in the legend.

measures in the top 20 features. For example, four graph measures were associated with the left middle temporal gyrus and left SMA.

3.2. Identifying hub nodes

As described in Section 2.6, we identified hub nodes in three groups of subjects, *i.e.* AD, MCI, and HC. Tables 6 and 7 list the in-degree and out-degree hub nodes for three groups, respectively. Fig. 4 shows the hub nodes of each group in the brain surface. As listed in Table 6, some hub nodes are common between three groups, namely ROIs 15, 76, 118, 233, and 256 which correspond to right parahippocampal gyrus, right insular cortex, left precuneus, left thalamus, and right precuneus, respectively. More importantly, some hub nodes are present only in HC group and they are missing in AD or MCI groups. These hub nodes are within the left parahippocampal gyrus and right inferior temporal gyrus. There are also some regions that were hub nodes in MCI and AD but not in HC. These regions were within the right calcarine fissure and right inferior parietal gyrus. Table 7 lists the hub nodes corresponding to the out-degree which are common in three groups.

4. Discussion

The main object of this study was to develop and evaluate an accurate method for automatic classification of AD, MCI, and HC based on rs-fMRI directed brain network analysis. Since MCI is an intermediate state between HC and AD, alterations of the brain network in patients with MCI as compared to either patients with AD or HC subjects may be relatively subtle, and thus achieving a high performance in discrimination of three groups is a challenging problem. We used various directed graph measures to investigate different aspects of the brain network integration, segregation, and centrality. Using these measures, we were able to identify differences between the brain networks of AD, MCI, and HC. The proposed algorithm in this study achieved an accuracy of 93.3% in discrimination of three groups (Table 2). An important factor in achieving this high discrimination accuracy was our consideration of the direction of connections of the brain network, calculated based on the Granger causality analysis.

Recently, we used graph measures calculated based on the undirected brain network, classified patients with MCI and AD from HC subjects, and achieved an accuracy of 88.4% [48], which is lower than the accuracy of the current study. The proposed method in the current study had specificity of 100% in identifying HC and AD and also sensitivity of 100% in identifying MCI (Tables 2 and 4). This means that the proposed method had 100% accuracy in identifying patients with MCI, and none of these patients was classified as either HC or AD. In addition, none of the patients with AD was classified as healthy controls and none of the healthy controls was classified as AD (Table 4). Furthermore, none of the patients with AD or MCI was classified as HC, and thus the proposed method had a false negative of zero in identifying patients with MCI or AD. This is a key feature of the proposed algorithm since classifying patients as healthy subject is a crucial limitation of an automatic diagnostic algorithm in clinical applications.

In our previous study for classification of AD, MCI, and HC using undirected graph measures [48], we found that the SVM and naïve Bayes classifier outperformed other classifiers. We also found that SVM outperformed the naïve Bayes classifier. In the current study for classification of AD, MCI, and HC using directed graph measures, our results revealed that the naïve Bayes classifier outperformed SVM in terms of accuracy, sensitivity, specificity, and positive predictivity. It is noteworthy that the naïve Bayes classifier has a clear advantage over the SVM with regard to the processing time.

Our results showed that the centrality graph measures (betweenness centrality and pagerank centrality) achieved best performance when used as a single feature for discrimination of three groups (Table 3). In fact, accuracy of classification of AD, MCI, and HC using only pagerank centrality or betweenness centrality resulted in 76.8% and 79.4%, respectively. Our results are in agreement with previous studies, [78], showing significant alteration of the betweenness centrality or pagerank centrality in patients with MCI and AD. In addition, some other studies, *e.g.* [6], reported that the eigenvector centrality, which is a variant of pagerank centrality, was a high discriminative feature in classification of patients with AD.

Classification performance of two parcellation approaches for defining nodes of the graph, *i.e.* the AAL and 264 putative functional areas atlases, is compared in Table 4. The accuracy of classification using the AAL atlas and the 264 putative functional areas atlas were 79.9% and 93.3%, respectively. The lower performance of the AAL atlas may be related to the fact that it parcels the brain based on an anatomical approach, which may not correspond to the functional brain organization. On the other hand, the 264 putative functional areas were defined based on functional brain networks and, thus, may be more sensitive to alterations of the brain functions in MCI and AD. In fact, previous studies have shown that functionally defined ROIs outperform the structurally defined ROIs in fMRI connectivity analysis, and provide better classification accuracy [48,80].

Results of the receiver operating characteristic (ROC) curves in Fig. 3 showed that: 1) our proposed method has a high performance for classification of HC *vs.* AD, HC *vs.* MCI, and MCI *vs.* AD; 2) the area under ROC curve (AUC) for classification of HC *vs.* AD was more than that of HC *vs.* MCI and MCI *vs.* AD. The later result is expected, since MCI is an intermediate state between HC and AD. These results suggest that the proposed machine learning approach based on the directed graph measures may serve as a biomarker for diagnosing MCI and AD.

Top 20 graph measures with most discrimination ability in Table 5 are mainly related to areas in the DMN which has been shown to be the main RSNs altered in various brain diseases, specifically in AD [10]. Discrimination abilities of the graph measures in corresponding areas were sorted in descending mode in Table 5, *i.e.* the graph measure on the top of the list has the most discrimination ability in identifying patients with AD and MCI from HC subjects. As listed in Table 5, the most affected area is the left middle temporal gyrus (ROI 97 in 264 putative functional area atlas). This

Table 4
Performance of classification using two parcellation approaches: AAL (90 areas) and 264 putative functional areas. AAL: automated anatomical labeling; 264: 264 putative functional areas; HC: healthy control; MCI: mild cognitive impairment; AD: Alzheimer's disease.

Atlas	Accuracy (%)	Group of subjects	Number of subjects as classified			Total number of subjects
			HC	MCI	AD	
264	93.29	HC	38	5	0	43
		MCI	0	88	0	88
		AD	0	6	27	33
AAL	79.88	HC	35	6	2	43
		MCI	7	78	3	88
		AD	6	9	18	33

Table 5
Top 20 features with the most discrimination ability between three groups of AD, MCI, and HC. These features were extracted in the feature selection step of proposed algorithm. The corresponding AAL area of each ROI in 264 putative functional area atlas is given in table.

Graph measure	ROI no	Resting-state network	Corresponding area in AAL atlas
In-degree	97	DMN	Left middle temporal gyrus
In-degree	130	DMN	Right medial superior frontal gyrus
Flow coefficient	258	Dorsal attention	Right superior parietal gyrus
Degree	62	Sensory/somatomotor Mouth	Right postcentral gyrus
Degree	244	Ventral attention	Left supplementary motor area
Strength	97	DMN	Left middle temporal gyrus
In-degree	209	Fronto-parietal Task Control	Right inferior temporal gyrus
Strength	244	Ventral attention	Left supplementary motor area
K-coreness centrality	62	Sensory/somatomotor Mouth	Right postcentral gyrus
Degree	97	DMN	Left middle temporal gyrus
Flow coefficient	207	Fronto-parietal Task Control	Right inferior frontal gyrus, triangular part
Flow coefficient	95	DMN	Left middle temporal gyrus
Flow coefficient	252	Dorsal attention	Left inferior parietal gyrus, excluding supramarginal and angular gyri
Local efficiency	165	Visual	Left superior occipital gyrus
Local efficiency	97	DMN	Left middle temporal gyrus
K-coreness centrality	244	Ventral attention	Left supplementary motor area
In-degree	65	Cingulo-opercular Task Control	Left rolandic operculum
PageRank centrality	165	Visual	Left superior occipital gyrus
Flow coefficient (number of paths)	258	Dorsal attention	Right superior parietal gyrus
In-degree	244	Ventral attention	Left supplementary motor area

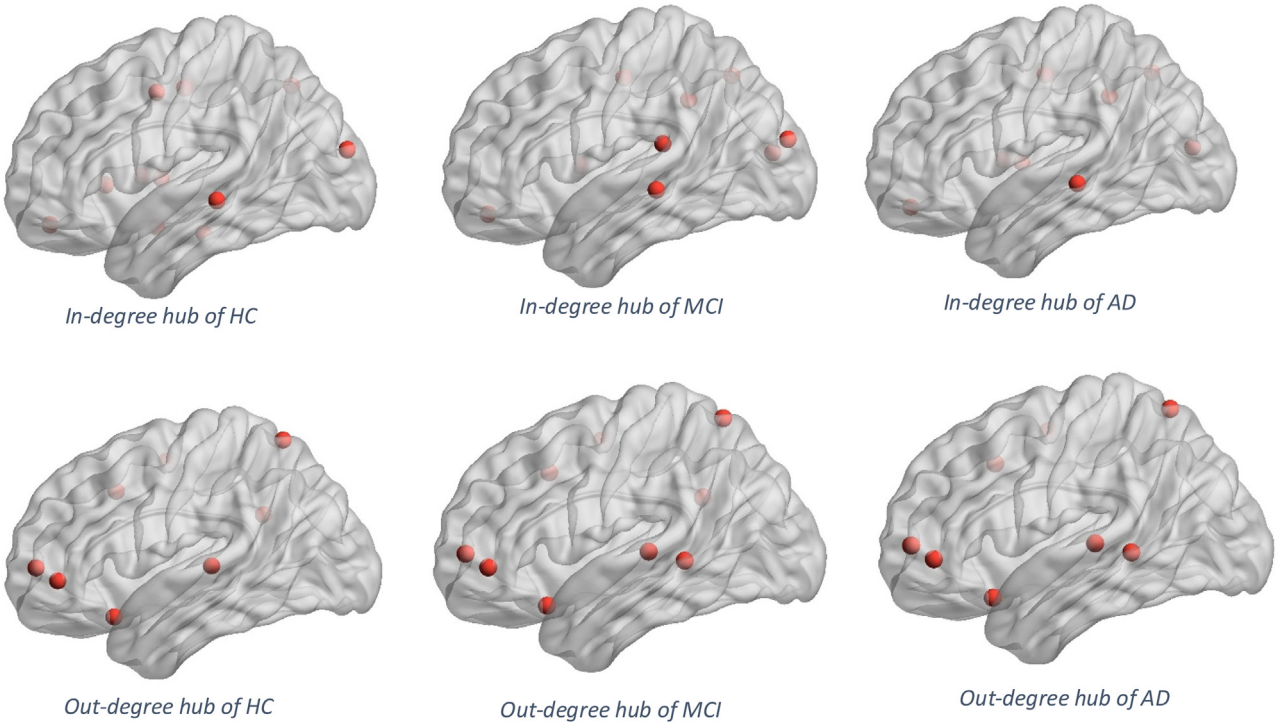

Fig. 4. Hub nodes in three groups of HC, MCI, and AD. Top row shows the in-degree hub nodes and the bottom row shows the out-degree hub nodes (See Tables 6 and 7). Only nodes with occurrence percentage higher than 70% in Tables 6 and 7 were shown. Plots of this figure were created using BrainNet Viewer [94].

Table 6
In-degree hub nodes identified in three groups of AD, MCI, and HC. Nodes with an in-degree of two standard deviation higher than the mean of in-degree of all nodes were identified as hub nodes. This analysis was repeated in different threshold values from 0.1 to 0.3 with a step of 0.01. Three columns on the right side of table represent percentage of occurrence of hubs in that ROI in a specific group (HC, MCI, and AD) across all 21 threshold values. The corresponding AAL area of each ROI in 264 putative functional area atlas is given in table.

	ROI no	Resting-state network	Corresponding area in AAL atlas	HC (%)	MCI (%)	AD (%)
Common hubs in HC, MCI and AD	15	–	Right parahippocampal gyrus	100	100	100
	76	Cingulo-opercular task control	Right insular cortex	100	100	100
	118	Default mode	Left precuneus	100	100	100
	233	Subcortical	Left thalamus	100	100	100
	256	Dorsal attention	Right precuneus	100	100	100
Common hubs in HC and MCI	149	Memory retrieval	Left precuneus	100	100	0
	16	–	Right lingual gyrus	100	48	0
	64	Cingulo-opercular task control	Left temporal pole: superior temporal gyrus	38	100	0
Common hubs in MCI and AD	169	Visual	Right calcarine fissure and surrounding cortex	0	100	71
	204	Fronto-parietal task control	Right inferior parietal gyrus, excluding supramarginal and angular gyri	0	100	86
Common hubs in HC and AD	123	Default mode	Right superior frontal gyrus, medial orbital	100	0	33
	234	Subcortical	Right thalamus	76	0	100
Hubs only in HC	9	–	Left parahippocampal gyrus	95	0	0
	209	Fronto-parietal task control	Right inferior temporal gyrus	100	0	0

Table 7
Out-degree hub nodes identified in three groups of AD, MCI, and HC. Nodes with an out-degree of two standard deviation higher than the mean of out-degree of all nodes were identified as hub nodes. This analysis was repeated in different threshold values from 0.1 to 0.3 with a step of 0.01. Three columns on the right side of table represent percentage of occurrence of hubs in that ROI in a specific group (HC, MCI, and AD) across all 21 threshold values. The corresponding AAL area of each ROI in 264 putative functional area atlas is given in table.

	ROI no	Resting-state network	Corresponding area in AAL atlas	HC (%)	MCI (%)	AD (%)
Common hubs in HC, MCI and AD	132	Default mode	Right superior frontal gyrus	100	100	100
	196	Fronto-parietal task control	Left medial superior frontal gyrus	100	100	100
	197	Fronto-parietal task control	Right superior frontal gyrus, orbital part	100	100	100
	198	Fronto-parietal task control	Right middle frontal gyrus	100	100	100
	263	Cerebellum	Vermis_6	100	100	100
	264	Cerebellum	Right Cerebelum_6	100	100	95
	66	Cingulo-opercular task control	Left insular cortex	100	100	90
	130	Default mode	Right medial superior frontal gyrus	100	100	33
	131	Default mode	Right precuneus	67	81	95

area is repeated four times in Table 5, corresponding to four graph measures, *i.e.* In-degree, strength, degree, and local efficiency. This result is in agreement with several studies that have reported the middle temporal gyrus as an important region in AD pathology [8,13,40,60,82]. Consistent with previous studies [22,69,96], we found that superior frontal gyrus, superior parietal gyrus, and supplementary motor area were affected in patients with AD or MCI (Table 5).

The top two discriminative features in Table 5 correspond to the in-degree graph measure and two regions within the DMN, namely left middle temporal gyrus and right medial superior frontal gyrus. This observation emphases the key role of these areas of the DMN in integrating information from other areas, and suggests alteration of this integration in patients with MCI and AD [59]. It can be seen from Table 5 that two features associated with the right postcentral gyrus and four features associated with the left supplementary motor area are among the top discriminative features. Consistent with these results, a previous study reported gradual loss of sensorimotor cortex with progression of AD [32], and functional alterations in sensorimotor areas in patients with AD have been reported in previous rs-fMRI studies [10,95].

Several studies have shown importance of hubs for understanding the brain disorders [20,62]. A study based on meta-analysis of structural MRI data in more than 20,000 subjects and 26 different brain disorders found that brain lesions which were common across all brain disorders were more likely to be located in hubs [17]. Specifically, this study found that patients with AD had lesions that were significantly more likely to be located in hubs, and in particular in temporal lobe hubs. Another study reported high levels of amyloid-β deposited in hub regions, and suggested that these regions are critical in the development of AD [11]. Since hub nodes integrate and distribute information, we included both in-degree and out-degree hubs in the current study and investigated alteration of the hub nodes in patients with MCI and AD. We found that the number of in-degree hubs in HC, MCI, and AD were 12, 10, and 9, respectively (Table 6), suggesting that patients with AD experience disappearing some hubs in their brain network during the progression of disease. We found that patients with MCI and AD did not have two in-degree hub regions, *i.e.* right inferior temporal gyrus (ITG) and left parahippocampal gyrus, though healthy subjects had these hubs. The ITG plays an essential role in verbal fluency and it has been shown that this region is affected in the early stage of AD [76]. The parahippocampal gyrus has consistently been reported as affected region in MCI and AD [60,85,88,96]. A meta-analysis of 121 structural and functional neuroimaging studies concluded that the hippocampus volume loss significantly discriminates between healthy subjects and patients with early AD [97]. The functional disconnection between the hippocampus and other brain regions in AD was also demonstrated [3].

As listed in Table 6, patients with AD were deficient in three hub regions, namely left precuneus (within the memory retrieval network), right lingual gyrus, and left temporal pole, whereas patients with MCI and HC subjects had these hubs. Lack of a hub node in the left temporal pole in patients with AD may relate to the naming impairment in these patients, which is associated with the left anterior temporal lobe (ATL) atrophy [26]. In fact, it has been suggested that the ATL serves as a hub for information processed in the distributed set of motor, sensory, and linguistic regions [66].

Lack of a hub node in the left precuneus in patients with AD may be associated with key role of this region in episodic memory, which is disrupted in AD [42,67,86]. The differences in hubs of patients with MCI and AD may be associated with the progressive trend of the disease from MCI to AD. In addition, compensatory effects in patients with MCI and AD may strengthen some connections and introduce new hub nodes. It has been shown that the functional connectivity between neighboring brain regions may not gradually decrease, instead, there is a severe decrease in MCI and then increase in AD [78]. In particular, patients with MCI who do not convert to AD (non-converters) have higher local and global efficiency in comparison with HC and MCI converters, which suggests a compensatory effect for the reduced cortical thickness in MCI non-converters as compared to HC [100].

It can be seen from Table 7 that hubs corresponding to the out-degree are mainly same in three groups. This finding suggests that the important brain regions that have strongest causal influence on the other regions are not highly affected in MCI and AD. This observation is in agreement with the results in Table 5 in which only in-degree and total degree features are among the top 20 discriminable features and there is no out-degree feature in this table. It is noteworthy that the selected features could be more specific for discriminating HC, MCI and AD if they were tested against random network measures. This issue should be investigated in future.

5. Conclusions

We integrated the directed graph measures with a machine learning approach on the basis of the rs-fMRI data to classify AD, MCI, and HC. The proposed algorithm was able to efficiently discriminate three groups with an accuracy of 93.3%. We identified optimal features with high discrimination ability and conducted hub node analysis to provide insights in the pathology of Alzheimer's disease. Granger causality analysis added information about the direction of connections in the brain network and facilitated the machine learning algorithm to perform a precise classification of AD, MCI, and HC.

Disclosure

None of the authors has any conflict of interest to disclose.

Acknowledgments

We thank Dr. Amanda Preston for her assistance with preparation of the manuscript.

Data used in this paper were obtained from the Alzheimer's Disease Neuroimaging Initiative (ADNI) database (http://ADNI.loni.usc.edu). The investigators within the ADNI, who can be found at http://ADNI.loni.usc.edu/study-design/ongoing-investigations, contributed to the design and implementation of ADNI and/or provided data but did not participate in analysis or writing of this article. Data collection and sharing for this project was funded by the Alzheimer's Disease Neuroimaging Initiative (ADNI) (National Institutes of Health Grant U01 AG024904). ADNI is funded by the National Institute on Aging, the National Institute of Biomedical Imaging and Bioengineering, and through generous contributions from the following: AbbVie, Alzheimer's Association; Alzheimer's Drug Discovery Foundation; Araclon Biotech; BioClinica, Inc.; Biogen; Bristol-Myers Squibb Company; CereSpir, Inc.; Eisai Inc.; Elan Pharmaceuticals, Inc.; Eli Lilly and Company; EuroImmun; F. Hoffmann-La Roche Ltd and its affiliated company Genentech, Inc.; Fujirebio; GE Healthcare; IXICO Ltd.; Janssen Alzheimer Immunotherapy Research & Development, LLC.; Johnson & Johnson Pharmaceutical Research & Development LLC.; Lumosity; Lundbeck; Merck & Co., Inc.; Meso Scale Diagnostics, LLC.; NeuroRx Research; Neurotrack Technologies; Novartis Pharmaceuticals Corporation; Pfizer Inc.; Piramal Imaging; Servier; Takeda Pharmaceutical Company; and Transition Therapeutics. The Canadian Institutes of Health Research is providing funds to support ADNI clinical sites in Canada. Private sector contributions are facilitated by the Foundation for the National Institutes of Health (www.fnih.org). The grantee organization is the Northern California Institute for Research and Education, and the study is coordinated by the Alzheimer's Disease Cooperative Study at the University of California, San Diego. ADNI data are disseminated by the Laboratory for Neuro Imaging at the University of Southern California.

References

[1] G.E. Alexander, K. Chen, P. Pietrini, S.I. Rapoport, E.M. Reiman, Longitudinal PET evaluation of cerebral metabolic decline in dementia: a potential outcome measure in alzheimer's disease treatment studies, Am. J. Psychiatry 159 (2002) 738–745.
[2] G. Allen, H. Barnard, R. McColl, A.L. Hester, J.A. Fields, M.F. Weiner, W.K. Ringe, A.M. Lipton, M. Brooker, E. McDonald, Reduced hippocampal functional connectivity in Alzheimer disease, Arch. Neurol. 64 (2007) 1482–1487.
[3] G. Allen, H. Barnard, R. McColl, A.L. Hester, J.A. Fields, M.F. Weiner, W.K. Ringe, A.M. Lipton, M. Brooker, E. McDonald, C.D. Rubin, C.M. Cullum, Reduced hippocampal functional connectivity in Alzheimer disease, Arch. Neurol. 64 (2007) 1482–1487.
[4] F. Bai, D.R. Watson, Y. Shi, Y. Wang, C. Yue, D. Wu, Y. Yuan, Z. Zhang, Specifically progressive deficits of brain functional marker in amnestic type mild cognitive impairment, PLoS One 6 (2011) e24271.
[5] F. Bai, Z. Zhang, H. Yu, Y. Shi, Y. Yuan, W. Zhu, X. Zhang, Y. Qian, Default-mode network activity distinguishes amnestic type mild cognitive impairment from healthy aging: a combined structural and resting-state functional MRI study, Neurosci. Lett. 438 (2008) 111–115.
[6] M.A. Binnewijzend, S.M. Adriaanse, W.M. Flier, C.E. Teunissen, J.C. Munck, C.J. Stam, P. Scheltens, B.N. Berckel, F. Barkhof, A.M. Wink, Brain network alterations in Alzheimer's disease measured by eigenvector centrality in fMRI are related to cognition and CSF biomarkers, Hum. Brain Mapp. 35 (2014) 2383–2393.
[7] K. Blennow, M.J. de Leon, H. Zetterberg, Alzheimer's disease, Lancet 368 (2006) 387–403.
[8] A. Bokde, P. Lopez-Bayo, T. Meindl, S. Pechler, C. Born, F. Faltraco, S. Teipel, H.-J. Möller, H. Hampel, Functional connectivity of the fusiform gyrus during a face-matching task in subjects with mild cognitive impairment, Brain 129 (2006) 1113–1124.
[9] P. Boldi, M. Santini, S. Vigna, PageRank: functional dependencies, ACM Trans. Inf. Syst. (TOIS) 27 (2009) 19.
[10] M.R. Brier, J.B. Thomas, A.Z. Snyder, T.L. Benzinger, D. Zhang, M.E. Raichle, D.M. Holtzman, J.C. Morris, B.M. Ances, Loss of intranetwork and internetwork resting state functional connections with Alzheimer's disease progression, J. Neurosci. 32 (2012) 8890–8899.
[11] R.L. Buckner, J. Sepulcre, T. Talukdar, F.M. Krienen, H. Liu, T. Hedden, J.R. Andrews-Hanna, R.A. Sperling, K.A. Johnson, Cortical hubs revealed by intrinsic functional connectivity: mapping, assessment of stability, and relation to Alzheimer's disease, J. Neurosci. 29 (2009) 1860–1873.
[12] E. Bullmore, O. Sporns, Complex brain networks: graph theoretical analysis of structural and functional systems, Nat. Rev. Neurosci. 10 (2009) 186–198.
[13] G.F. Busatto, G.E. Garrido, O.P. Almeida, C.C. Castro, C.H. Camargo, C.G. Cid, C.A. Buchpiguel, S. Furuie, C.M. Bottino, A voxel-based morphometry study of temporal lobe gray matter reductions in Alzheimer's disease, Neurobiol. Aging 24 (2003) 221–231.
[14] K.A. Celone, V.D. Calhoun, B.C. Dickerson, A. Atri, E.F. Chua, S.L. Miller, K. DePeau, D.M. Rentz, D.J. Selkoe, D. Blacker, Alterations in memory networks in mild cognitive impairment and Alzheimer's disease: an independent component analysis, J. Neurosci. 26 (2006) 10222–10231.
[15] E. Challis, P. Hurley, L. Serra, M. Bozzali, S. Oliver, M. Cercignani, Gaussian process classification of Alzheimer's disease and mild cognitive impairment from resting-state fMRI, Neuroimage 112 (2015) 232–243.
[16] Y. Chao-Gan, Z. Yu-Feng, DPARSF: a MATLAB toolbox for pipeline data analysis of resting-state fMRI, Front. Syst. Neurosci. 4 (2010) 13.
[17] N.A. Crossley, A. Mechelli, J. Scott, F. Carletti, P.T. Fox, P. McGuire, E.T. Bullmore, The hubs of the human connectome are generally implicated in the anatomy of brain disorders, Brain 137 (2014) 2382–2395.
[18] R. Cuingnet, E. Gerardin, J. Tessieras, G. Auzias, S. Lehéricy, M.-O. Habert, M. Chupin, H. Benali, O. Colliot, A.s.D.N. Initiative, Automatic classification of patients with Alzheimer's disease from structural MRI: a comparison of ten methods using the ADNI database, Neuroimage 56 (2011) 766–781.
[19] C. Davatzikos, P. Bhatt, L.M. Shaw, K.N. Batmanghelich, J.Q. Trojanowski, Prediction of MCI to AD conversion, via MRI, CSF biomarkers, and pattern classification, Neurobiol. Aging 32 (2011), 2322. e2319–2322. e2327.

[20] W. de Haan, K. Mott, E.C. van Straaten, P. Scheltens, C.J. Stam, Activity dependent degeneration explains hub vulnerability in Alzheimer's disease, PLoS Comput. Biol. 8 (2012) e1002582.
[21] X. Delbeuck, M. Van der Linden, F. Collette, Alzheimer' disease as a disconnection syndrome? Neuropsychol. Rev. 13 (2003) 79–92.
[22] B. Desgranges, J.-C. Baron, B. Giffard, G. Chételat, C. Lalevée, F. Viader, V. de la Sayette, F. Eustache, The neural basis of intrusions in free recall and cued recall: a PET study in Alzheimer's disease, Neuroimage 17 (2002) 1658–1664.
[23] G. Deshpande, Z. Li, P. Santhanam, C.D. Coles, M.E. Lynch, S. Hamann, X. Hu, Recursive cluster elimination based support vector machine for disease state prediction using resting state functional and effective brain connectivity, PLoS One 5 (2010) e14277.
[24] S.I. Dimitriadis, N.A. Laskaris, V. Tsirka, M. Vourkas, S. Micheloyannis, S. Fotopoulos, Tracking brain dynamics via time-dependent network analysis, J. Neurosci. Methods 193 (2010) 145–155.
[25] P. Domingos, M. Pazzani, On the optimality of the simple Bayesian classifier under zero-one loss, Mach. Learn. 29 (1997) 103–130.
[26] K. Domoto-Reilly, D. Sapolsky, M. Brickhouse, B.C. Dickerson, A.s.D.N. Initi, Naming impairment in Alzheimer's disease is associated with left anterior temporal lobe atrophy, Neuroimage 63 (2012) 348–355.
[27] R.O. Duda, P.E. Hart, D.G. Stork, Pattern Classification, Wiley, 2001.
[28] G. Fagiolo, Clustering in complex directed networks, Phys. Rev. E 76 (2007) 026107.
[29] M.D. Fox, A.Z. Snyder, J.L. Vincent, M. Corbetta, D.C. Van Essen, M.E. Raichle, The human brain is intrinsically organized into dynamic, anticorrelated functional networks, Proc. Natl. Acad. Sci. U. S. A. 102 (2005) 9673–9678.
[30] R. Franciotti, N.W. Falasca, L. Bonanni, F. Anzellotti, V. Maruotti, S. Comani, A. Thomas, A. Tartaro, J.-P. Taylor, M. Onofrj, Default network is not hypoactive in dementia with fluctuating cognition: an Alzheimer disease/dementia with Lewy bodies comparison, Neurobiol. Aging 34 (2013) 1148–1158.
[31] P. Fransson, Spontaneous low-frequency BOLD signal fluctuations: an fMRI investigation of the resting-state default mode of brain function hypothesis, Hum. Brain Mapp. 26 (2005) 15–29.
[32] G.B. Frisoni, A. Prestia, P.E. Rasser, M. Bonetti, P.M. Thompson, In vivo mapping of incremental cortical atrophy from incipient to overt Alzheimer's disease, J. Neurol. 256 (2009) 916–924.
[33] K.J. Friston, C.D. Frith, R.S. Frackowiak, R. Turner, Characterizing dynamic brain responses with fMRI: a multivariate approach, Neuroimage 2 (1995) 166–172.
[34] K.A. Garrison, D. Scheinost, E.S. Finn, X. Shen, R.T. Constable, The (in) stability of functional brain network measures across thresholds, Neuroimage 118 (2015) 651–661.
[35] J. Geweke, Measurement of linear dependence and feedback between multiple time series, J. Am. Stat. Assoc. 77 (1982) 304–313.
[36] C.W. Granger, Investigating causal relations by econometric models and cross-spectral methods, Econometrica: J. Econometric Soc. (1969) 424–438.
[37] M.D. Greicius, B. Krasnow, A.L. Reiss, V. Menon, Functional connectivity in the resting brain: a network analysis of the default mode hypothesis, Proc. Natl. Acad. Sci. 100 (2003) 253–258.
[38] M.D. Greicius, G. Srivastava, A.L. Reiss, V. Menon, Default-mode network activity distinguishes Alzheimer's disease from healthy aging: evidence from functional MRI, Proc. Natl. Acad. Sci. U. S. A. 101 (2004) 4637–4642.
[39] P. Hagmann, L. Cammoun, X. Gigandet, R. Meuli, C.J. Honey, V.J. Wedeen, O. Sporns, Mapping the structural core of human cerebral cortex, PLoS Biol. 6 (2008) e159.
[40] Y. He, Z. Chen, A. Evans, Structural insights into aberrant topological patterns of large-scale cortical networks in Alzheimer's disease, J. Neurosci. 28 (2008) 4756–4766.
[41] J.L. Hellerstein, T. Jayram, I. Rish, Recognizing end-user transactions in performance management, IBM Thomas J. Watson Res. Div. (2000).
[42] K. Herholz, E. Salmon, D. Perani, J.C. Baron, V. Holthoff, L. Frolich, P. Schonknecht, K. Ito, R. Mielke, E. Kalbe, G. Zundorf, X. Delbeuck, O. Pelati, D. Anchisi, F. Fazio, N. Kerrouche, B. Desgranges, F. Eustache, B. Beuthien-Baumann, C. Menzel, J. Schroder, T. Kato, Y. Arahata, M. Henze, W.D. Heiss, Discrimination between Alzheimer dementia and controls by automated analysis of multicenter FDG PET, Neuroimage 17 (2002) 302–316.
[43] C.J. Honey, R. Kötter, M. Breakspear, O. Sporns, Network structure of cerebral cortex shapes functional connectivity on multiple time scales, Proc. Natl. Acad. Sci. 104 (2007) 10240–10245.
[44] C.R. Jack, M.A. Bernstein, N.C. Fox, P. Thompson, G. Alexander, D. Harvey, B. Borowski, P.J. Britson, J. L Whitwell, C. Ward, The alzheimer's disease neuroimaging initiative (ADNI): MRI methods, J. Magn. Reson. Imaging 27 (2008) 685–691.
[45] B. Jie, D. Zhang, H.-I. Suk, C.-Y. Wee, D. Shen, Integrating multiple network properties for MCI identification, in: Machine Learning in Medical Imaging, Springer, 2013, pp. 9–16.
[46] B. Jie, D. Zhang, C.Y. Wee, D. Shen, Topological graph kernel on multiple thresholded functional connectivity networks for mild cognitive impairment classification, Hum. Brain Mapp. 35 (2014) 2876–2897.
[47] A. Kelly, L.Q. Uddin, B.B. Biswal, F.X. Castellanos, M.P. Milham, Competition between functional brain networks mediates behavioral variability, Neuroimage 39 (2008) 527–537.
[48] A. Khazaee, A. Ebrahimzadeh, A. Babajani-Feremi, Application of advanced machine learning methods on resting-state fMRI network for identification of mild cognitive impairment and Alzheimer's disease, Brain Imaging Behavi. (2015) 1–19.
[49] A. Khazaee, A. Ebrahimzadeh, A. Babajani-Feremi, Application of pattern recognition and graph theoretical approaches to analysis of brain network in alzheimer's disease, J. Med. Imaging Health Inf. 5 (2015) 1145–1155.
[50] A. Khazaee, A. Ebrahimzadeh, A. Babajani-Feremi, Identifying patients with Alzheimer's disease using resting-state fMRI and graph theory, Clin. Neurophysiol. 126 (2015) 2132–2141.
[51] S. Kintali, 2008. Betweenness centrality: Algorithms and lower bounds. arXiv preprint arXiv:0809.1906.
[52] S. Klöppel, C.M. Stonnington, C. Chu, B. Draganski, R.I. Scahill, J.D. Rohrer, N.C. Fox, C.R. Jack, J. Ashburner, R.S. Frackowiak, Automatic classification of MR scans in Alzheimer's disease, Brain 131 (2008) 681–689.
[53] W. Koch, S. Teipel, S. Mueller, J. Benninghoff, M. Wagner, A.L. Bokde, H. Hampel, U. Coates, M. Reiser, T. Meindl, Diagnostic power of default mode network resting state fMRI in the detection of Alzheimer's disease, Neurobiol. Aging 33 (2012) 466–478.
[54] V. Latora, M. Marchiori, Efficient behavior of small-world networks, Phys. Rev. Lett. 87 (2001) 198701.
[55] R. Li, J. Yu, S. Zhang, F. Bao, P. Wang, X. Huang, J. Li, Bayesian network analysis reveals alterations to default mode network connectivity in individuals at risk for Alzheimer's disease, PLoS One 8 (2013) e82104.
[56] Y. Li, Y. Qin, X. Chen, W. Li, Exploring the functional brain network of Alzheimer's disease: based on the computational experiment, PLoS One 8 (2013) e73186.
[57] P. Liang, Z. Li, G. Deshpande, Z. Wang, X. Hu, K. Li, Altered causal connectivity of resting state brain networks in amnesic MCI, PLoS One 9 (2014) e88476.
[58] P. Liang, Z. Wang, Y. Yang, K. Li, Three subsystems of the inferior parietal cortex are differently affected in mild cognitive impairment, J. Alzheimer's Dis. 30 (2012) 475–487.
[59] W. Liao, J. Ding, D. Marinazzo, Q. Xu, Z. Wang, C. Yuan, Z. Zhang, G. Lu, H. Chen, Small-world directed networks in the human brain: multivariate Granger causality analysis of resting-state fMRI, Neuroimage 54 (2011) 2683–2694.
[60] F. Liu, C.-Y. Wee, H. Chen, D. Shen, Inter-modality relationship constrained multi-modality multi-task feature selection for Alzheimer's Disease and mild cognitive impairment identification, Neuroimage 84 (2014) 466–475.
[61] Z. Liu, Y. Zhang, L. Bai, H. Yan, R. Dai, C. Zhong, H. Wang, W. Wei, T. Xue, Y. Feng, Y. You, J. Tian, Investigation of the effective connectivity of resting state networks in Alzheimer's disease: a functional MRI study combining independent components analysis and multivariate Granger causality analysis, NMR Biomed. 25 (2012) 1311–1320.
[62] V. Menon, Developmental pathways to functional brain networks: emerging principles, Trends Cogn. Sci. 17 (2013) 627–640.
[63] X. Miao, X. Wu, R. Li, K. Chen, L. Yao, Altered connectivity pattern of hubs in default-mode network with Alzheimer's disease: an Granger causality modeling approach, PLoS One 6 (2011) e25546.
[64] T.M. Mitchell, R. Hutchinson, R.S. Niculescu, F. Pereira, X. Wang, M. Just, S. Newman, Learning to decode cognitive states from brain images, Mach. Learn. 57 (2004) 145–175.
[65] M.E. Newman, Assortative mixing in networks, Phys. Rev. Lett. 89 (2002) 208701.
[66] K. Patterson, P.J. Nestor, T.T. Rogers, Where do you know what you know? The representation of semantic knowledge in the human brain, Nat. Rev. Neurosci. 8 (2007) 976–987.
[67] S.E. Perez, B. He, M. Nadeem, J. Wuu, S.W. Scheff, E.E. Abrahamson, M.D. Ikonomovic, E.J. Mufson, Resilience of precuneus neurotrophic signaling pathways despite amyloid pathology in prodromal Alzheimer's disease, Biol. Psychiatry 77 (2015) 693–703.
[68] R.C. Petersen, G.E. Smith, S.C. Waring, R.J. Ivnik, E.G. Tangalos, E. Kokmen, Mild cognitive impairment: clinical characterization and outcome, Arch. Neurol. 56 (1999) 303–308.
[69] S.G. Potkin, G. Alva, D. Keator, D. Carreon, K. Fleming, J.H. Fallon, Brain metabolic effects of Neotrofin in patients with Alzheimer's disease, Brain Res. 951 (2002) 87–95.
[70] J.D. Power, A.L. Cohen, S.M. Nelson, G.S. Wig, K.A. Barnes, J.A. Church, A.C. Vogel, T.O. Laumann, F.M. Miezin, B.L. Schlaggar, S.E. Petersen, Functional network organization of the human brain, Neuron 72 (2011) 665–678.
[71] Z. Qi, X. Wu, Z. Wang, N. Zhang, H. Dong, L. Yao, K. Li, Impairment and compensation coexist in amnestic MCI default mode network, Neuroimage 50 (2010) 48–55.
[72] I. Rish, J. Hellerstein, J. Thathachar, An analysis of data characteristics that affect naive Bayes performance, IBM T. J. Watson Res. Center 30 (2001).
[73] S.A. Rombouts, F. Barkhof, R. Goekoop, C.J. Stam, P. Scheltens, Altered resting state networks in mild cognitive impairment and mild Alzheimer's disease: an fMRI study, Hum. Brain Mapp. 26 (2005) 231–239.
[74] M. Rubinov, O. Sporns, Complex network measures of brain connectivity: uses and interpretations, Neuroimage 52 (2010) 1059–1069.
[75] M. Rubinov, O. Sporns, Weight-conserving characterization of complex functional brain networks, Neuroimage 56 (2011) 2068–2079.
[76] S.W. Scheff, D.A. Price, F.A. Schmitt, M.A. Scheff, E.J. Mufson, Synaptic loss in the inferior temporal gyrus in mild cognitive impairment and Alzheimer's disease, J. Alzheimers Dis. 24 (2011) 547–557.
[77] G. Schwarz, Estimating the dimension of a model, Ann. Stat. 6 (1978) 461–464.

[78] E.H. Seo, D.Y. Lee, J.M. Lee, J.S. Park, B.K. Sohn, D.S. Lee, Y.M. Choe, J.I. Woo, Whole-brain functional networks in cognitively normal, mild cognitive impairment, and Alzheimer's disease, PLoS One 8 (2013) e53922.
[79] A.K. Seth, A MATLAB toolbox for Granger causal connectivity analysis, J. Neurosci. Methods 186 (2010) 262–273.
[80] W.R. Shirer, S. Ryali, E. Rykhlevskaia, V. Menon, M.D. Greicius, Decoding subject-driven cognitive states with whole-brain connectivity patterns, Cereb. Cortex 22 (2012) 158–165.
[81] C. Sorg, V. Riedl, M. Mühlau, V.D. Calhoun, T. Eichele, L. Läer, A. Drzezga, H. Förstl, A. Kurz, C. Zimmer, Selective changes of resting-state networks in individuals at risk for Alzheimer's disease, Proc. Natl. Acad. Sci. 104 (2007) 18760–18765.
[82] C. Stam, B. Jones, G. Nolte, M. Breakspear, P. Scheltens, Small-world networks and functional connectivity in Alzheimer's disease, Cereb. Cortex 17 (2007) 92–99.
[83] N. Tzourio-Mazoyer, B. Landeau, D. Papathanassiou, F. Crivello, O. Etard, N. Delcroix, B. Mazoyer, M. Joliot, Automated anatomical labeling of activations in SPM using a macroscopic anatomical parcellation of the MNI MRI single-subject brain, Neuroimage 15 (2002) 273–289.
[84] M.P. van den Heuvel, O. Sporns, Network hubs in the human brain, Trends Cogn. Sci. 17 (2013) 683–696.
[85] P.J. Visser, P. Scheltens, F.R. Verhey, B. Schmand, L.J. Launer, J. Jolles, C. Jonker, Medial temporal lobe atrophy and memory dysfunction as predictors for dementia in subjects with mild cognitive impairment, J. Neurol. 246 (1999) 477–485.
[86] A.D. Wagner, B.J. Shannon, I. Kahn, R.L. Buckner, Parietal lobe contributions to episodic memory retrieval, Trends Cogn. Sci. 9 (2005) 445–453.
[87] J. Wang, X. Zuo, Z. Dai, M. Xia, Z. Zhao, X. Zhao, J. Jia, Y. Han, Y. He, Disrupted functional brain connectome in individuals at risk for Alzheimer's disease, Biol. Psychiatry 73 (2013) 472–481.
[88] L. Wang, Y. Zang, Y. He, M. Liang, X. Zhang, L. Tian, T. Wu, T. Jiang, K. Li, Changes in hippocampal connectivity in the early stages of Alzheimer's disease: evidence from resting state fMRI, Neuroimage 31 (2006) 496–504.
[89] Z. Wang, P. Liang, X. Jia, Z. Qi, L. Yu, Y. Yang, W. Zhou, J. Lu, K. Li, Baseline and longitudinal patterns of hippocampal connectivity in mild cognitive impairment: evidence from resting state fMRI, J. Neurol. Sci. 309 (2011) 79–85.
[90] D.J. Watts, S.H. Strogatz, Collective dynamics of 'small-world'networks, Nature 393 (1998) 440–442.
[91] C.-Y. Wee, P.-T. Yap, K. Denny, J.N. Browndyke, G.G. Potter, K.A. Welsh-Bohmer, L. Wang, D. Shen, Resting-state multi-spectrum functional connectivity networks for identification of MCI patients, PLoS One 7 (2012) e37828.
[92] W.W.-S. Wei, Time Series Analysis, Addison-Wesley publ., Reading, 1994.
[93] X. Wen, X. Wu, R. Li, A.S. Fleisher, E.M. Reiman, X. Wen, K. Chen, L. Yao, Alzheimer's disease-related changes in regional spontaneous brain activity levels and inter-region interactions in the default mode network, Brain Res. 1509 (2013) 58–65.
[94] M. Xia, J. Wang, Y. He, BrainNet Viewer: a network visualization tool for human brain connectomics, PLoS One 8 (2013) e68910.
[95] M. Xia, Z. Wang, Z. Dai, X. Liang, H. Song, N. Shu, K. Li, Y. He, Differentially disrupted functional connectivity in posteromedial cortical subregions in Alzheimer's disease, J. Alzheimer's Dis. 39 (2014) 527–543.
[96] Z. Yao, Y. Zhang, L. Lin, Y. Zhou, C. Xu, T. Jiang, A.s.D.N. Initiative, Abnormal cortical networks in mild cognitive impairment and Alzheimer's disease, PLoS Comput. Biol. 6 (2010) e1001006.
[97] K.K. Zakzanis, S.J. Graham, Z. Campbell, A meta-analysis of structural and functional brain imaging in dementia of the Alzheimer's type: a neuroimaging profile, Neuropsychol. Rev. 13 (2003) 1–18.
[98] Z. Zhang, L. Deng, F. Bai, Y. Shi, H. Yu, Y. Yuan, K. Wang, T. Jiang, J. Jia, Z. Zhang, Alteration of resting brain function by genetic variation in angiotensin converting enzyme in amnestic-type mild cognitive impairment of Chinese Han, Behav. Brain Res. 208 (2010) 619–625.
[99] Z. Zhang, Y. Liu, T. Jiang, B. Zhou, N. An, H. Dai, P. Wang, Y. Niu, L. Wang, X. Zhang, Altered spontaneous activity in Alzheimer's disease and mild cognitive impairment revealed by Regional Homogeneity, Neuroimage 59 (2012) 1429–1440.
[100] Y. Zhou, Y.W. Lui, Small-World properties in mild cognitive impairment and early alzheimer's disease: a cortical thickness MRI study, ISRN Geriatr. 2013 (2013) 542080.